Networked web-cameras monitor congruent seasonal development of birches with phenological field observations

Mikko Peltoniemi[1,*], Mika Aurela[2], Kristin Böttcher[3], Pasi Kolari[4], John Loehr[5], Tatu Hokkanen[1], Jouni Karhu[1], Maiju Linkosalmi[2], Cemal Melih Tanis[2], Sari Metsämäki[3], Jukka-Pekka Tuovinen[2], Timo Vesala[4], Ali Nadir Arslan[2]

1 Natural Resources Institute Finland (Luke), Latokartanonkaari 9, FIN-00790, Helsinki, Finland

2 Finnish Meteorological Institute, Erik Palménin aukio 1, FI-00560,

3 Finnish Environment Institute (SYKE), Mechelininkatu 34a, FIN-00251 Helsinki, Finland

4 Department of Physics, PO Box 68, 00014 University of Helsinki

5 Lammi Biological Station, University of Helsinki, Pääjärventie 320, 16900 Lammi, Finland

*Corresponding author: Mikko Peltoniemi, mikko.peltoniemi@luke.fi, tel. + 358 40 801 5329, Latokartanonkaari 9, FIN-00790, Helsinki, Finland

Abstract

Ecosystems' potential to provide services, e.g. to sequester carbon, is largely driven by the phenological cycle of vegetation. Timing of phenological events is required for understanding and predicting the influence of climate change on ecosystems and to support analyses of ecosystem functioning. Analyses of conventional camera time series mounted near vegetation has been suggested as a means of monitoring phenological events and supporting wider monitoring of phenological cycle of biomes that is frequently done with satellite earth observation (EO). Especially in the boreal biome, sparsely scattered deciduous trees amongst conifer-dominant forests pose a problem for EO techniques as species phenological signal mix, and render EO data difficult to interpret. Therefore, deriving phenological information from on the ground measurements would provide valuable reference data for earth observed phenology products in a larger scale. Keeping this in mind, we established a network of digital cameras for automated monitoring of phenological activity of vegetation in the boreal ecosystems of Finland. Cameras were mounted at 14 sites, each site having 1-3 cameras. In this study, we used data from 12 sites to investigate how well networked cameras can detect the phenological development of birches (*Betula spp.*) along a latitudinal gradient. Birches typically appear in small quantities within the dominant species. We tested whether the small, scattered birch image elements allow a reliable extraction of colour indices and the temporal changes therein. We compared automatically derived phenological dates from these birch image elements both to visually determined dates from the same image time series and to independent observations recorded in the phenological monitoring network covering the same region. Automatically extracted season start dates, which were based on the change of green colour fraction in spring, corresponded well with the visually interpreted start of the season, and also to the budburst dates observed in the field. Red colour fraction turned out to be superior to the green colour-based indices in predicting leaf yellowing and fall. The latitudinal gradients derived using automated phenological date extraction corresponded well with the gradients estimated from the

phenological field observations. We conclude that small and scattered birch image elements allow reliable extraction of key phenological dates for the season start and end of deciduous species studied here, providing thus important species-specific data for model validation and for explaining the temporal variation in EO phenology products.

Keywords: birch, budburst, camera, monitoring, phenology, time lapse

1 Introduction

Timing of spring onset has advanced significantly during the last century (Menzel et al., 1999, Menzel et al., 2006, Delbart et al., 2008, Jeong et al., 2011, Zhao et al., 2015). Seasonal variation of vegetation activity directly affects photosynthesis, growth of trees and plant reproductive investment, so it is an important driver of the global carbon balance and thus is strongly linked to climate change (Hogg et al., 2000, Richardson et al., 2013). A recent study that compared phenological data to predictions of 36 tree phenology models showed that both inter-annual and spatial variations of phenology is poorly predicted by the models (Basler et al., 2016). This is critical as the year-to-year variation in the timing of budburst of birches (*Betula* spp.) in the boreal zone varies in a wide range of 40 days (Häkkinen, 1999). Poor reproduction of the phenological cycle in biosphere models has also been shown to cause a consistent overestimation of carbon balance in comparison to measured data (Richardson et al., 2012, 2013). The predictive power of models can be expected to further degrade under climate change, due to decoupling of light and temperature cycles. Decoupling of these cycles will be pronounced in northern latitude forests, which are expected to face increases of mean temperatures by 2-7 ˚C (Ruosteenoja et al., 2016). Therefore, continuous, long-term monitoring of vegetation activity is needed.

Phenological monitoring has a long tradition, and phenological observation networks exist in many countries across the world (Siljamo et al., 2008). At the same time, many spectro- and radiometric instruments suitable for phenological monitoring are operating from space, complementing the dating of phenological events over wider regions (Zhang et al. 2006, Böttcher et al., 2014, Gonsamo et al., 2016). In recent years, also near-surface remote sensing with time lapse imaging (Richardson et al., 2007) has provided a cost-effective methodology to monitor and ground-truth phenological phenomena (Hufkens at al., 2012, Klosterman et al., 2014). Time lapse imaging solves some of the problems associated with traditional field observations, as more quantitative methods can be used to define the start of the growing season, for example, while still maintaining the link to the visual appearance of

plants. Time-lapse image based phenological development could also provide a closer analogy to remote sensing than field observations of phenology, which are not fully comparable with remote sensing observations as they detect different traits (Badeck et al., 2004). Methodologically, automated curve fitting and transition date extraction methods used for camera image time series have similarities with EO data processing (Elmore et al., 2014; Klosterman et al., 2014).

Cameras have most often been used to analyse the phenological development of deciduous species (Richardson et al., 2007), although also other types of ecosystems, such as grasslands (e.g. Migliavacca et al., 2011), peatlands (Westergaard-Nielsen et al., 2013, Peichl et al., 2015, Linkosalmi et al., 2016) and coniferous forests (Nagai et al., 2012, Linkosalmi et al., 2016), have been monitored. Analyses are robust to the scene illumination angle, cloud cover and camera type, if suitable analysis methods are used (Sonnentag et al., 2012; Linkosalmi et al., 2016; Peltoniemi et al., 2017). Colour changes in plant tissue are unlikely to occur without a biochemical or biophysical mechanism, and digital photography has provided insight into these mechanisms (Keenan et al., 2014; Yang et al., 2014). For deciduous species, budburst and leaf senescence events and also their relationship with CO_2 exchange have been in a focus in a number of studies, and these phenomena have been analysed with various colour indices (Richardson et al., 2007, Ahrends et al., 2009, Sonnentag et al., 2012, Mizunuma et al., 2013, Wingate et al., 2015).

There are still open questions regarding how the camera-derived phenological data should be used in an optimal way. It would be interesting to know how the image-extracted dates compare with those based on the field definitions used in phenological observation networks, and which transition dates can be extracted with sufficient accuracy. This would provide more solid basis for using cameras to supplement existing field observation networks. Secondly, a single image may provide a wealth of information on several species, some only appearing in the margins of the image or amidst the dominant vegetation in

smaller proportions and the understory, but the use of such information has been rare. Still, the non-dominant elements potentially provide important information for interpreting earth observations, which aggregate information from an area that may not be fully represented by the species dominating the camera view (Hufkens et al., 2012). In the boreal zone, deciduous trees often occur in relatively small and fragmented areal proportions in the satellite footprint. While the areal proportion may be small, their phenology causes distinctive changes in the reflective properties of canopies (Böttcher et al., 2014; Jönsson et al., 2010), which complicates phenological analyses of conifers, and may even render results unreliable.. Species-specific phenological information drawn from image time series combined with high-resolution earth observation data on species distributions could markedly improve the quality of satellite-based phenology estimation (Liang et al., 2011; Liu et al.2015). If part of the monitoring would be based on scattered and smaller species-specific image elements, and not only camera views dominated by species, the cost of representative monitoring of wide area phenology would naturally be reduced.

We established a network of cameras at 14 boreal sites in Finland, each including 1-3 cameras in different positions. Most of the sites in the network are dominated by Scots pine (*Pinus sylvestris)* and Norway spruce (*Picea abies*), and some are peatlands. Twelve of the sites have a varying mixture of *Betula spp.,* allowing a cross-site study of their phenology, and making it possible to study how these sometimes small and marginal image elements of widely distributed species could benefit phenological monitoring using web-cameras.

The objectives of this study were to test the use of the recently established camera network for birch phenology analysis and supplementing existing phenological field observations. We were interested in how selected color indices compare to the conventional phenological observations, and whether the scattered and often small birch elements within the images provide a useful source of information for

the phenology analysis. The tests were performed by comparing the phenological transition dates extracted from the image time series to the corresponding visual estimates, and to those observed in the field in the frame of phenological observation network of Finland, which covers a long latitudinal transect ranging from 60°N to nearly 70°N (Poikolainen et al., 1996; Pudas et al., 2008).

2 Materials and Methods

2.1 Sites and camera installations

Camera sites cover nearly the full range of climatic variations observed in Finland, their location ranging from the hemiboreal Tvärminne to the sub-arctic Kaamanen (Figure 1, Table 1). Three of the northern sites are wetlands [Sodankylä wetland, Kaamanen, Lompolojänkkä Integrated Carbon Observation System (ICOS) sites] and two are dominated by *P. sylvestris* (Scots Pine)(Sodankylä ICOS site, Värriö), and one by *Picea abies* L. Karst (Norway spruce) (Kenttärova, ICOS site). The Paljakka site in central Finland is dominated by spruce and it belongs to the long-term phenology monitoring network of Luke, as does the mixed species site Parkano in southern Finland. The other southern sites are dominated by *P. sylvestris* (Hyytiälä ICOS site), *Picea abies* L. Karst (Punkaharju, Tammela Level II monitoring sites of the International Co-operative Programme on Assessment and Monitoring of Air Pollution Effects on Forests, ICP), or have mixed or deciduous coverage (Tvärminne, Lammi Long Term Ecosystem Research (LTER) sites). The sites vary in their ancillary measurements, the most intensively measured sites being the ICOS sites in Hyytiälä and Sodankylä while the Suonenjoki *P. sylvestris* site only hosts a meteorological station.

Table 1 Cameras and sites used in this study, the total numbers of pixels analysed for each site, and DOI to original image time series. Coordinates are in decimal degrees WGS84.

No.	Site	Lat.	Lon.	Camera view / dominant species	Species	Spring periods in data	Autumn period in data	Pixels in target ROI	DOI[2]
1	Hyytiälä (crown)	61.85	24.30	Forest canopy / *P. sylvestris*	*B. pendula*	2014-2016	2014-2016	26695[1]	10.5281/zenodo.815559
2	Kaamanen	69.14	27.27	Wetland / *Sphagnum spp.*	*B. pubescens*	2015-2016	2015 – (2016)	39527	10.5281/zenodo.815553
3	Kenttärova (canopy)	67.99	24.24	Forest canopy / *P. abies*	*B. pubescens*	2015-2016	2015-2016	51370	10.5281/zenodo.815519
4	Lammi	61.0	25.0	Mixed	*B.*	2016	2016	59865	10.5281/zenodo.81554

	(landscape)	5	4	landscape / *B. pendula*	*pendula*			0	2
5	Lompolojänkkä	69.80	24.21	Wetland / grasses	*B. pubescens*	2015	2015	324728	10.5281/zenodo.815555
6	Paljakka	64.68	64.68	Mixed landscape / *P. abies*	*B. pubescens*	2016	2015	16867	10.5281/zenodo.815529
7	Parkano	62.03	23.04	Mixed landscape / *B. pendula*	*B. pendula*	2016	2015-2016	487184	10.5281/zenodo.815487
8	Sodankylä, wetland	67.37	26.65	Wetland / *Sphagnum spp.*	*B. pubescens*	2014-2015	2014-2016	64076	10.5281/zenodo.815485
9	Suonenjoki	62.64	27.05	Forest crown level / *P. sylvestris*	*B. pendula*	2016	2015-2016	155758	10.5281/zenodo.815489
10	Tammela (canopy)	60.65	23.81	Forest canopy / *P. abies*	*B. pendula*	2014-2016	2014-2016	46022	10.5281/zenodo.815450
11	Tvärminne	59.84	23.25	Mixed landscape / *P. sylvestris*	*B. pendula*	2016	2016	77705	10.5281/zenodo.815550
12	Värriö (crown)	67.75	29.61	Forest crown level / *P. abies*	*B. pubescens*	2015-2016	2016	191423	10.5281/zenodo.815534
	N site-years					20	21		

1 Hyytiälä crown camera had resolution 1024 x 768 while others had 2594 x 1944.

2 Peltoniemi et al., 2017

All cameras are set to a fixed white balance, quarter of the maximum resolution (5 MPix), targeted northwards where feasible and triggered for half-hourly submission of snapshots to an ftp server, excluding the night hours. All of the sites and analyses of this study used image time series acquired with StarDot NetCam SC5 cameras.

2.2 Phenological analyses

Material for phenological analyses

In this study, we used 12 networked cameras for the analyses of spring and autumn phenology of *Betula* spp from 2014-2016. Installation and operation dates of the cameras varied, and not every camera covered the whole period. Some cameras had suffered from damages or mounting failures, and had been reinstalled causing gaps in time series. Therefore, depending on the availability of images at the camera site during this period, we analysed the phenology of either a full year or a limited spring or autumn period, as indicated in Table 1.

The ROIs were selected subjectively to cover the sub-regions that best represented the birch crowns within the camera view (Appendix A). Consequently, ROIs varied in shape, size and the number of sub-polygons defining the ROI, depending on the features and number of suitable targets. The number of sub-polygons varied from 1 to 6 per image time series, the ROIs most often representing individual trees in the images.

Targeted crowns in the ROI also had a variable background, depending on whether there were conifer crowns, peatland vegetation or sky in the background of the targeted crown. Some of the targets were large and had a uniform background, while others were small and had uniform background. Based on preliminary analysis, we excluded two targets that had seedling birches against an understory vegetation background, to avoid risk confusing two distinctive sources of vegetation signals, and one target with a single distant birch tree against conifers (excluded partly due to camera movement). The remaining unclear cases were analysed in order to study if their phenological transition dates are plausible with respect to other sites' results and other materials. For these purposes, targets were classified either as distant-small and near-clear, and effects of category tested in Anova (see below).

For each ROI, we calculated the mean green chromatic coordinate (GCC) and red chromatic coordinate (RCC) as GCC = G / (R + G + B) and RCC = R / (R + G + B)], where R, G, and B, and pixel red, green, and blue channel digital numbers, respectively. For the extraction of digital numbers from images, and the calculation of these indices, we used a custom made program (FMIPROT, Tanis et al., submitted).

The pixels of ROIs with poor or excess exposure were excluded from the GCC calculation; we used only pixels with digital numbers between 30 and 254, to avoid too dim and overexposed pixels and their non-linear effects on GCC and RCC. The use of R, G and B threshold therefore eliminated images from the darkest periods in winter in northern Finland.

The image time series consisted of half-hourly images that were taken within the daily period of 8:00-16:00 UTC+2. From all images available for a day, and for all days, we calculated daily medians of GCC and RCC, which were used in subsequent analyses. We also calculated daily 90^{th} upper percentiles, but as our preliminary analysis showed that the median provided less noisy (but otherwise very similar) results, we used the daily medians in the final analyses.

Turning point estimation from continuous color indexes: phenological transition dates

We fitted continuous curves to the GCC and RCC data (daily medians), which allowed the estimation of turning points that correspond to the transition dates. The curve fits were made between DOY 90 (Mar 1^{st}) and 310 (Oct 6^{th}), except for the northernmost Kaamanen site, where we started the fits on DOY 125 (Mar 25^{th}), and the second northernmost Värriö site, where we ended the fit period on DOY 300 (Sep 27^{th}). Focusing the fits on these periods eliminated the infection of colour signals by canopy snow cover

and dark winter days, which can bias the signal and add variation to GCC (Linkosalmi et al., 2016), and thus negatively influence the curve fitting and subsequent extraction of GCC transition dates. Any gaps in the GCC time series, due to low light or camera malfunctioning, were filled with linear interpolation.

We fitted different versions of double logistic functions (Gu et al., 2009, Elmore et al., 2012, Klosterman et al., 2014) to the GCC data. The formulation by Gu et al. (2009) produced curves that systematically fitted well to the data. While the methods of Klosterman et al. (2014) and Elmore et al. (2012) typically produced good fits, but sometimes they produced very poor fits. This was likely because Klosterman et al. (2014) and Elmore et al. (2012) included more parameters than Gu et al. (2009), which made the regression more unstable. Therefore in subsequent analyses, we only used the method of Gu et al. (2009) as implemented in *phenopix* (Filippa et al., 2016), which fits the function of the following form:

$$GCC(t) = y_0 + \frac{a_1}{\left[1+e^{\left(-b_1^{-1}(t-t_{01})\right)}\right]^{c_1}} - \frac{a_2}{\left[1+e^{\left(-b_2^{-1}(t-t_{02})\right)}\right]^{c_2}} \quad (1)$$

where GCC(t) is the GCC median of day t, and y_0, a_1, b_1, c_1, t_{01}, a_2, b_2, c_2, and t_{02} are parameters to be estimated. The equation is composed of two modified logistic functions that characterize increasing and decreasing parts of the season. The function is flexible, but may omit finer variation of season progression. The uncertainty of fits and subsequent estimation of transition date estimates (see below) was made with a method implemented in GuFit() function of the phenopix library, i.e. by repeating the fit 100 times by introducing uncertainty to the observations.

Statistical performance of the double exponential fits was evaluated and compared by calculating the root mean squared deviation (RMSD) by site and year as RMSD = $(\text{sum}((g_i\text{-}p_i)/n))^{½}$ where i is day, g is the observed GCC, p is the modelled GCC, and n is the number of days. The median and the 2.5 and 97.5

230 percentiles of RMSD were estimated for each site-year combination from the ensemble of 100 fits so as
231 to evaluate the uncertainty of fits.
232
233 We also used *SplineFit()* function from the *phenopix* R library (Filippa et al., 2016) to fit cubic spline
234 regressions to the daily time series of GCC and RCC (Filippa et al., 2016). The fit is sensitive to the
235 selection of the degree of freedom of the fit (parameter *k*). We allowed the fit algorithm to select the
236 optimum *k* automatically. We also made preliminary tests of the effects of *k* selection to the fits and
237 subsequent transition date estimation, but found out that the varied k values around the optimal *k*
238 produced very similar estimates of season transition dates, and hence report only the fits and transition
239 dates with the optimal *k*. RMSD was estimated similarly as with the double-logistic fit.
240
241 We extracted phenological transition dates from the fitted curves with the *PhenoExtract()* function of
242 the *phenopix* library. For spline fits, we used the '*derivatives'* method that extracts the dates when the
243 GCC increase is steepest in the spring (SOS, start of season) and when the autumnal decrease in GCC is
244 steepest (EOS, end of season), as implemented in the *greenbrown* R library (Forkel et al., 2015, Forkel
245 and Wutzler 2015). The date of the maximum GCC during the season was denoted as POP (peak of
246 season). Additionally, we estimated the end of season from the peak of spline smoothed RCC (EOSr, end
247 of season RCC). The methods for estimating the transition dates are shortly described in

248 Table 2. For the double logistic fit using the method presented by Gu et al. (2009), we extracted the
249 transition dates estimating the first marks of fractional increase of green color (GCC) of leaves (UD,
250 upturn date), the stabilization date of this fraction to summer levels (SD, stabilization date), the first
251 marks of autumn decline (DD, downturn date), and the levelling of GCC to late autumn levels (RD,
252 recession date).

253 Table 2 Automatically estimated phenological transition dates from image time series.

Acronym	Variable name	Explanation	Reference

DD	Downturn date	Intersection of horizontal lines through summer GCC plateau and line tangential to the peak senescing point that is estimated from the minimum of the first derivative of GCC.	(Gu et al., 2009); (Filippa et al., 2016)
EOS	End of season (from GCC)	Midpoint of the autumn senescence period, defined as the maximum of the first derivative of the senescing curve. Used for spline fitted seasonal development.	(Forkel et al., 2015); (Forkel and Wutzler 2015)
EOSr	End of season (from RCC)	Maximum of the spline fitted RCC curve in the autumn.	-
POP	Peak of season	Maximum of the spline fitted GCC curve in the season.	(Filippa et al., 2016)
SOS	Start of season	Used for spline fitted seasonal development.	(Forkel et al., 2015); (Forkel and Wutzler 2015)
RD	Recession date	Intersection of horizontal lines through autumn minimum GCC and line tangential to the peak senescing point that is estimated from the minimum of the first derivative of GCC. Occurs generally when leaves grow fast in the spring.	(Gu et al., 2009); (Filippa et al., 2016)
SD	Stabilization date	Intersection of horizontal lines through summer GCC plateau and line tangential to the peak recovery point that is estimated from the maximum of the first derivative of GCC.	(Gu et al., 2009); (Filippa et al., 2016)
UD	Upturn date	Intersection of horizontal lines through spring minimum GCC and line tangential to the peak recovery point that is estimated from the maximum of the first derivative of GCC. Occurs generally when leaves grow fast in the spring.	(Gu et al., 2009); (Filippa et al., 2016)

Phenological field observations

We used a subset of data for years 2015-2016 from the phenological field observation network operating in Finland (Poikolainen et al., 1996; Pudas et al., 2008). The number of locations in this subset was 17 and the sites covered the latitudinal domain of phenology cameras (Table 3, Figure 1). At each stand the observations were made individually by observing five medium-sized and healthy birches.

Table 3 Phenological field observation sites used in the study.

ID	Site	Latitude	Longitude	Species
a	Aulanko	61.02	24.46	*B. pubescens*
b	Joensuu	62.6	29.73	*B. pubescens & B. pendula*
c	Kannus	63.93	23.89	*B. pubescens & B. pendula*
d	Kevo	69.76	27.01	*B. pubescens*
e	Kolari	67.35	23.83	*B. pubescens & B. pendula*

f	Lapinjarvi	60.62	26.17	*B. pubescens & B. pendula*
g	Muddusjarvi	69.06	27.11	*B. pubescens*
h	Muhos	64.82	26.01	*B. pubescens & B. pendula*
i	Oulanka	66.35	29.32	*B. pubescens & B. pendula*
j	Parkano	62.03	23.04	*B. pubescens & B. pendula*
k	Preitila	60.45	22.76	*B. pubescens & B. pendula*
l	Punkaharju	61.81	29.33	*B. pubescens & B. pendula*
m	Ruotsinkyla	60.36	24.99	*B. pubescens & B. pendula*
n	Solbole	60.04	23.04	*B. pubescens & B. pendula*
o	Suonenjoki	62.64	27.06	*B. pendula*
p	Varrio	67.75	29.61	*B. pubescens & B. pendula*
q	Vesijako	61.39	25.05	*B. pubescens & B. pendula*

According to the field guide of the network (Kubin et al., 2007), the budburst date ('Budburst') was recorded when half of the leaves of *Betula* spp.have emerged from the bud. However, these leaves have not yet unfolded, i.e. the blade and midrib of leaves are not yet visible. The guide complements this definition by stating that at budburst the trees show the first marks of green colour in spring from a distance. We compared these dates to imagesextracted UD and SOS.

An estimate of the date when leaves have grown to full size and thickness ('Leaves grown') was recorded when there was no apparent increase in size or thickness of the individual leaves of the crown. At this time crowns of birches usually have also reached their full density. We compared these dates to image extracted SD.

The leaf yellowing date ('Leaves yellow') was defined as the date when 50% of individual crowns have yellow leaves due to the normal autumnal senescence process, and not due to diseases such as leaf rust fungi. We compared these dates to image extracted EOSr.

The leaf fall date ('Leaves fallen') was defined as the date when 50% of leaves of individual tree crowns had shed leaves.

Visual transition estimates from image time series

Using turning point analysis we also compared the transition dates extracted from the image time series to the visually determined season transition dates from the same image time series, so as to verify how well the automated analysis is able to detect transition dates and periods determined visually by going through image time series (half-hourly images). When several targets were available from an observation site, the means of all trees of focal species were recorded to visually determine the transition dates. This also corresponds to the automatically extracted GCC that were estimated either as a mean of several polygons if several trees of same species were present, or as a mean of a wider image area of homogeneous canopy.

An experienced phenological observer, who had no other association with the data analyses, developed and used a protocol for detecting birch leaf budburst, maturation and leaf autumn colouring from image time series. The observer followed, as closely as possible, the same field guidance as was used within the phenological observation network (Kubin et al., 2007), although obvious modifications were introduced due to the low resolution of images and, in some cases, distant elements. The estimation of the budburst date of *Betula* spp. relied on the colour change of the tree crowns, as it was rarely possible to distinguish individual leaves. This definition presumably yields results that are very close to those from the observation network, which also takes note of the colour change of the canopy from a distance. We compared these budburst estimates to UD and SOS.

An image-based estimate corresponding to the 'Leaves grown' estimate of the observation network was defined as the date when the birch crowns have reached their full density. After this date the crowns start to lose their distinctive light green colour. We compared these estimates to SD and POP.

Instead of a single date corresponding to the leaf yellowing date, we estimate a period during which leaves turn yellow, so as to better quantify the correspondence with the automatically estimated DD and RD. These dates were defined as the date at which 10% and 90% of leaves are yellow or brown, and it was assumed that the field-observed date when 50% of leaves were yellow occurs between these dates. A similar approach was used to estimate the leaf fall period (10% and 90% fallen). These dates presumably contained the field-observed date (when 50% of leaves had fallen), had we had a direct field observation of the imaged trees. We also compared these dates to EOS and EOSr.

Statistical comparisons and effect analyses

Irradiance conditions have been earlier found to influence GCC of conifers, rendering images useless when it is too dark (Linkosalmi et al., 2016). We studied if radiation and temperature can explain day-to-day variation in GCC data, e.g. by exposing different and a variable number of pixels for the GCC or RCC calculation of the ROI depending mostly on the light available to the inner canopy, or by influencing camera image cell sensitivity, respectively. Given that day-to-day variation of midday irradiance and temperature can be large in comparison to slower pace shifts occurring in phenology, the absence or small contribution of these variables would indicate that they are unlikely to influence the analyses of derived transition dates. Alternatively, a large effect of these variables would indicate that irradiance changes bias the transition date estimates based on image time series.

In order to estimate how large an effect light conditions and temperature can have on the GCC detected with the cameras, we fitted a linear mixed effects model with a temporal autocorrelation (AR1) term. Because GCC values are not comparable across sites, we scaled them by site and year to have mean of zero and unit standard deviation. The AR1 structure removes the trend-like variation in GCC by assuming that residuals of the model are auto-correlated, meaning that previous day's GCC is accounted for in the

prediction of the present GCC, which evidently clears the data from seasonal changes of GCC. The model formulation makes it possible to estimate the direct effects of light conditions and temperature on the present GCC. The fitted model form was

$$y_{ijt} = a_0 + a_1 T_{ijt} + a_2 G_{ijt} + a_3 G_{ijt} \times T_{ijt} + b_{0i} u_{s_i} + b_{1ij} u_{Y_{ij}} + \varphi_{ij} y_{ij(t-1)} + e_{ijt}, \quad (2)$$

where y is the GCC observation, and subscripts i, j, and t denote the site, year, and day of the observation, respectively. Fixed terms included the intercept (a_0) and daily mean temperature (T) and global radiation (G), and interaction of T and G, with respective coefficients a_1, a_2, and a_3. For T and G we used spatially downscaled estimates made for the nearest grid point (Venäläinen et al., 2005). The model has intercepts b_{0i} and b_{1ij} for random terms u for sites (s) and years (Y), respectively. Autocorrelation was modelled with AR1 process having an autocorrelation coefficient φ. The model was fitted with the *lme* function of the R package *nlme* (Pinheiro et al., 2015). The model was fitted to a selected subset of the data including Hyytiälä (2014-2016), Kenttärova, Sodankylä and Tammela (2015-2016), Kaamanen (2015), and Tvärminne and Värriö and Lammi (2016), which all had full time series from UD-10 to RD+10 days.

For testing the relationship of GCC and RCC based estimates and the estimates based on visual interpretations of corresponding transition dates, we plotted 1:1 graphs, fitted linear models between the estimates and estimated their mutual correlation coefficient. We also used linear mixed effects models to estimate the significance of differences between the transition dates (UD, SOS, EOSr) estimated with different methods. Method types included GCC (or RCC) based estimation, visual

interpretation, and field observation. Field observation was not conducted at camera sites, so we also included latitude (and year) in this regression. The transition date y_{it} estimated with these methods was modelled as

$$y_{it} = a_0 + a_1 l_i + a_2 Y_{it} + a_3 l_i \times Y_{it} + a_4 E_{it} + b_{0i} u_{s_i} + e_{it} \quad (3)$$

where a_0 is the intercept, a_1, $a_{1,}$ and a_2 are the coefficients for l_i is the latitude (easting (m) of the Finland Uniform Coordinate System) of the site and Y_{ij} (year), and their interaction, respectively. E_{ij} is the method of the observation of the observation, having a_3 as its coefficient. Coefficients b_{0i} are for the random terms u for sites s_i, and e_{it} is the normally distributed error. We also estimated separate linear regressions to investigate the latitudinal relationships of transition dates obtained from cameras and the field observation network. All statistical analyses were made in R (R Core Team, 2015).

3 Results

Fits to GCC and RCC data

Double logistic fits replicated the upturn of the GCC response at season start for the birch ROI at Lammi (Appendix A, Figure 2) and the other sites as well as the spline regression (Appendixes A and B). However, the slope of the senescing trail of GCC after the season peak varied by site and year, and double logistic function did not always fit to shapes of the trails (Appendix B). The parametrically more flexible spline regressions were able to catch the whole seasonal course of GCC and had better RMSD than double logistic fits (0.00172 vs, 0.00216, seeAppendix C). However, being sensitive to within season variation of GCC, it sometime falsely interpreted season end from GCC data (EOS) (Figure 2). For the season end date, estimates obtained for red peak (EOSr) of the spline smoothed RCC were always plausible (Figure 3, Appendix B).

For double logistic fit, the uncertainty of transition date extraction varied. Uncertainty ranges of UD, SD, and RD (10th - 90th percentile range) were on average 1.0, 1.4, and 2.5 d, respectively, while for DD it was 5.6 d.

Based on the autocorrelation model (Eq. 1), radiation had small, yet significant, effect on the observed day-to-day GCC variation (Table 4). Altogether, the fixed covariates (temperature, radiation and their interaction) were able to explain 1.6% of day-to-day variation of GCC (average across site-years).

Table 4 Results of the model (fixed terms) explaining day-to-day variation in GCC (scaled to zero mean and unit standard deviation) with daily mean temperature (T, °C) and radiation sum (G, MJ m^{-2} day^{-1}), and their interaction. φ is the autocorrelation coefficient of the AR1 autocorrelation structure.

	Dependent variable:
	GCC
a_0 (intercept)	-0.27
	(0.17)

a_1 (T)	0.0014
	(0.0036)
a_2 (G)	-0.0120***
	(0.0030)
a_3 (G x T)	0.00068***
	(0.00021)
φ	0.97
Observations	2317
Log Likelihood	-221.38
Akaike Inf. Crit.	458.77
Bayesian Inf. Crit.	504.75
Note:	*p<0.1; **p<0.05; ***p<0.01

391

392 None of the transition dates, nor the length of green-up period (SD-UD) or season (EOSr-SOS) were
393 explained by the type of the ROI (distant and small vs. near and clear) as analysed by linear mixed
394 effects models with and without the latitude covariate (all p > 0.05, models not shown, for data see
395 Appendix C).

396

397 *Comparison of season start estimates*

398 The estimates of transition dates for start of the season (SOS) were significantly related to the visually
399 estimated budburst date (Figure 3), but they were on average 6.37 days later than the visual estimate
400 and field observation of the budburst date (Table 5).

401

402 The upturn date (UD) was also significantly associated with the budburst date (Figure 4**Error! Reference**
403 **source not found.**). The camera-observed UD was on average 3.46 and 4.08 days ahead of the visual and
404 field observed budburst (Table 5). It is notable that the estimation of UD was occasionally interfered
405 with by the preceding snowmelt that occurred in the background of the birch targets (Kenttärova and
406 Värriö), which reduced the correlation.

407

The visual estimates of budburst were mostly between the estimated UD and SOS dates (16 out of 19 cases where they could be compared) (Appendix C Table C.3).

Comparison of season end estimates

The autumn peak of RCC (EOSr) was clearly associated with the visual season end estimates (90% of canopy yellow) (Figure 3). EOSr also associated with the date when 90% of leaves were interpreted as fallen from the tree crowns. EOS was less clearly associated with these events than EOSr (Figure 4). We found no statistical evidence that EOSr would be different from the visually interpreted leaf yellowing date (Table 5).

DD and RD dates were weakly related to dates when 10% and 90% leaves were yellow or fallen.

Comparison of midseason estimates

POP was related with canopy maturation (leaves grown) but the relationship deteriorated with increasing DOY for the northern sites (Figure 3).

SD was correlated with the visual estimate of the date of full-sized leaves but on average was dated earlier (Figure 4).

Table 5 Model of transition dates with latitude, with method and year of observation as covariates. Yellowing date in field was recorded when 50% canopy was yellow, while visual camera based observations were made when 90% of the canopy was yellow. Interaction between the latitude and observation type were insignificant and not included in the models ($p>0.05$). $^{*}p<0.1$; $^{**}p<0.05$; $^{***}p<0.01$. Note, latitudinal slope is composed of two species, *B. pubescent* in north and *B. pendula* in south.

Camera-based estimate	UD	SOS	EOSr
Field/Vis. Observation	Budburst	Budburst	Leaves yellow
Intercept (camera, 2015)	-18.43	-7.81	439.71***
	(12.62)	(12.82)	(23.52)
Latitude (km)	2.14***	2.14***	-2.47***
	(0.18)	(0.18)	(0.33)

Year 2016	-5.17***	-6.24***	-8.03***
	(0.76)	(0.81)	(1.26)
Field obs.	4.08***	-6.41***	-1.26
	(1.26)	(1.29)	(2.32)
Visual obs.	3.46***	-6.37***	1.12
	(1.12)	(1.18)	(1.74)
Observations	89	90	82
Log Likelihood	-243.77	-251.28	-263.08
Akaike Inf. Crit.	501.53	516.56	540.15
Bayesian Inf. Crit.	518.55	533.66	556.56
Note:	*p<0.1; **p<0.05; ***p<0.01		

Latitudinal gradients of transition dates

Our camera network made it possible to determine the latitudinal gradient in transition dates across Finland. There was a clear south-north trend in the season lengths (Figure 6), the seasons becoming shorter by 4.81 (±0.63 Std. Err.) days per 100 km when moving northwards (Table 6). This trend was caused by a later start (both SOS and UD) and earlier end (EOSr) of the season in the north, which increased by 2.07 (± 0.42; for UD 1.94 ± 0.40) and decreased by 2.77 (± 0.52; for SD 2.18±0.49) days per 100 km northwards, respectively, in year 2016. The latitudinal slopes were not statistically different between the years (Figure 7, Table 6, tested during Table 6 analyses). There were no differences between latitudinal trends of field observations and the corresponding GCC and RCC-based estimates (UD and budburst, SOS and budburst, and EOSr and yellowing; interactions were not significant, not shown). POP and RD also had significant latitudinal relationships, but EOS and SD did not (Appendix C.3). Interestingly, the residual standard errors (RSEs) of the camera derived latitudinal relationships for SOS

449 and UD were almost as small as those of the field observed budburst date, and EOSr and SD had even a

450 smaller RSE than the field observed leaf fall date.

451

452 Table 6 Latitude relationships of the phenological transition dates of season. Budburst and yellowing
453 dates are estimated from field observations in the phenological network in Finland. Others are extracted
454 from image time series. Values in parentheses are standard errors of estimates. *p<0.1; **p<0.05;
455 ***p<0.01. Units of dependent variables are numbers of days for EOSr-SOS and DOY for others. Note,
456 latitudinal slopes are composed of two species, *B. pubescent* in north and *B. pendula* in south.

	Dependent variable (DOY)						
	EOSr-SOS	SOS	EOSr	UD	SD	Budburst	Yellowing
Intercept (2016)	462.73***	-10.41	453.74***	-8.66	-13.53	11.48	468.20***
	(44.82)	(30.03)	(37.08)	(28.28)	(35.25)	(19.05)	(35.76)
Lat. (100 km)	-4.81***	2.07***	-2.77***	1.94***	2.18***	1.69***	-3.01***
	(0.63)	(0.42)	(0.52)	(0.40)	(0.49)	(0.27)	(0.50)
2015	37.38	20.08	27.44	-22.38	-24.77	-36.01	-52.38
	(71.44)	(47.07)	(57.53)	(47.23)	(53.63)	(26.13)	(48.57)
Lat:2015	-0.56	-0.13	-0.27	0.38	0.53	0.59	0.86
	(0.99)	(0.65)	(0.80)	(0.65)	(0.75)	(0.37)	(0.69)
Observations	17	19	19	18	20	52	43
R^2	0.90	0.83	0.79	0.82	0.83	0.74	0.65
Adjusted R^2	0.87	0.80	0.75	0.78	0.80	0.72	0.63
Residual Std. Error	7.51	5.04	6.21	4.74	5.91	4.51	7.72
F Statistic	38.23***	24.99***	18.76***	20.67***	26.66***	45.07***	24.59***
Note:	*p<0.1; **p<0.05; ***p<0.01						

457

458

459

460

4 Discussion

We used our newly established digital camera network (Peltoniemi et al., 2017) for assessing birch phenology along a latitudinal transect across Finland. We showed that the network is useful for monitoring birch phenology, although the site-specific analyses often relied on appearances of small birches among other vegetation and in different types of positions and environments. This stems from the fact that birch phenological colour changes were distinctive enough to be discerned from background and sometimes small targets.

The networked cameras were particularly useful for detecting the start of the growing season green-up and the autumnal leaf yellowing. According to our results, UD is able to capture even minor changes in crown greenness and to date those reliably, on average, UD estimates season start less than 4 days earlier than the budburst date recorded in the field. This is close to what has been earlier observed for ash and beech in Switzerland (Ahrends et al., 2008) and for 13 deciduous sites in eastern North America (Klosterman et al., 2014). On the other hand, SOS systematically dates the season start approximately 6 days later than the visual and field-based observations and thus provides a reasonable late estimate, suggesting that the season start should be calculated as the mean of the UD and SOS dates. For typical seasonal paths of GCC, the extraction of these dates seems to be fairly insensitive to day-to-day variation of GCC.

Season end was best estimated with the RCC peak (EOSr) in the autumn, which compared well with the visually interpreted dates of season end. In practice, we showed no bias of EOSr relative to the date when 90% leaves were yellow. The indices based on GCC (DD, RD, EOS) turned out to be useless for the prediction of season end.

There are various sources of uncertainty in the analyses. Generally, the uncertainties of curves depicting the season progression, and extractions of key transition dates were surprisingly small. For double logistic fits, considerable uncertainties were quantified for a few cases where the automated extraction of transition dates were challenging due to the nature of the analysed GCC time series [Appendix B, due to unexplained variation of GCC (for SD in Sodankylä 2014), slowly declining season (for DD and or RD: Hyytiälä, Kenttärova 2016, Paljakka 2015, Suonenjoki 2015 and 2016), or limited availability of data in spring (for SD: Paljakka 2016, Suonenjoki 2015)]. Otherwise, the typical daily mean GCC data seems to well support the extraction of transition dates, and considerable uncertainties seem to exist elsewhere than in curve fits and date extractions. This applies also to the spline fits whereby date extractions at least partially require subjective selection of smoothing parameter.

Challenges in discerning spring dates may also arise when conditions in the background of canopies change considerably during or before budburst. Snow melt in the background of target trees appears to be the most important factor in this region for biasing the season start estimates. For Värriö site UD occurred earlier (11.5-13.3 d, depending on year) than the visual observation, which is more than the average lag across sites (3.5 d). However, for SOS there seemed to be no significant snow induced bias (Appendix C). For further improvement of extraction algorithms, snow cover changes in the background of targets should be accounted for, either by more careful selection of the targets or by introducing a snow detection algorithm (Salvatori et al., 2011, Garvelmann et al., 2013; Arslan et al., 2017). Use of cameras in conjunction with high-resolution satellite imagery for the detection of the presence of snow in the vicinity of a camera could resolve some of the challenges. For instance, Sentinel-2 MSI provides an excellent data source for this and we have an already implemented method (SCAmod, Metsämäki et al., 2015) for deriving information about snow cover in 10m spatial resolution. Use of far and near remote

sensing methods together would provide spatially) and temporally complementary material, and could yield better performing snow and seasonal indices..

In our case, conifer background of birch targets had a minor effect on the GCC signal, as GCC and the extracted transition dates were in good accord with the transition dates that were visually assessed from the image time series (without any prior knowledge of GCC development) (Suppl. B). During the budburst of birches, the vegetation in the image background is rarely active, as conifers are not yet developing new shoots, which makes it easy to distinguish the GCC changes due to birch leaf growth. Co-occurring GCC changes of conifers (Wingate et al., 2015) potentially associated with photosynthetic and/or pigment recovery of conifer seem to be small in comparison to GCC changes caused by birch leaf growth. Possibly, phenological date extraction of midseason phenological phases could benefit from incorporation of background subtraction using mixing models (Keenan et al., 2013).

For colour index analyses, the small image elements were sufficient. However, small movement of the cameras at Sodankylä wetland site caused particularly uncertain transition date estimates during 2014 (Suppl. B), although the resulting transition date estimates did not differ from the main trends in other data. The images omitted from the analysis contained a site where unexpected movement of the camera mast would have obscured the analysis of small and distant targets. These problems may be partially due to defining too narrow ROI or ROI with too small safety margin to other targets, which exposes the view to variable set of pixels as the targets move due to wind, and in the longer term due to growth. Distance from camera to target, on the other hand, tends to even out colour differences. In our work, we did not find clear effects of colours of distant elements being obscured to the extent it would have hampered the analysis, but it could be problematic in locations with more frequent occurrence of excess condensation of air humidity moisture or fogs.

535 Other simultaneous phenological events in trees could potentially confound the season start estimation
536 from images. Flowering of birch occurs nearly simultaneously with budburst, with some variation in the
537 timing between individual birch trees. As a typical masting tree species, the annual variation of the
538 amount of male and female flowers of birches can be enormous. In a good flowering year, usually those
539 with high May temperatures, the amount of catkins is usually several thousands in a single birch (Ranta
540 et al. 2008, Zamorano et al. 2016). Birch flowering appears brownish and blurry in distant images. GCC
541 changes due to increased brown tones likely remain small, but large numbers of flowers during masting
542 years may render small changes of GCC more difficult to discern, and thus could cause a small delay of
543 UD estimates on those years. For some other species, however, flowering may cause more problems,
544 and the use of SOS could be a better option.
545
546 Comparisons between cameras and field data are also complicated by uncertainties of field
547 observations. We did not have camera-observed estimates of phenology from the same trees and years
548 as the ones available from the phenological observation network, and therefore we compared different
549 datasets when investigating the latitudinal gradient. Therefore, it is important to understand how
550 birches in individual sites represent the other birches in the same latitude. Clearly, the best camera-
551 based transition date estimates (UD, EOSr) were within the variation in the dates estimated from the
552 field observations (Figure 7), although on average a few days earlier and later, respectively. Siljamo et al.
553 (2008) found out that individual sites represent *Betula* spp. season start dates with an accuracy of 3-8
554 days as compared to the regional means, with northern locations such as Finland having smaller
555 uncertainties. At a single site, our field observations showed that the budburst date varied among tree
556 individuals of the same *Betula* spp. by 1.1 days (average of site std. dev. among individuals) and the
557 yellowing and fall dates by 3 days within the same year. Obviously, such differences are partly driven by
558 genetic variability among individuals (Rousi and Pusenius, 2005) and partly due to variation in the
559 growth environment of the trees, for example trees in open environments or surrounded by other

deciduous trees experience earlier budburst in comparison to trees among conifers due to higher sun exposure. Some of the field observations were made very close to the cameras (at Parkano, Paljakka, Värriö, Hyytiälä and Suonenjoki), suggesting that the uncertainties at these sites are smaller than that estimated by Siljamo et al. (2008), likely closer to the lower 3 day boundary of Siljamo et al., 2008. Uncertainties due to field observations themselves are hard to assess, as the visual assessment is subjective, albeit informed by guidelines and conducted by experienced personnel. It should also be noted that the visual interpretation by expert observers from image time series gave similar results to field observations, which implies that the uncertainties of subjective observations may not be critical for the conclusions of our study about the usefulness of UD, SOS and EOSr for phenological monitoring. Further investigations on how well transition dates extracted from image time series represent the definitions used in particular observation networks obviously require data collection from the same trees as monitored for phenology.

Analyses of season stabilization (SD) were less successful than those of UD, SOS, and EOSr, and the deviations from the corresponding visual estimate (leaves grown) were larger, as also others have found (Klosterman et al., 2014). This may be partly due to the less precise observation of the date when leaves were grown to their full size in the field and more difficult interpretation of the image time series. GCC also saturate immediately when leaves cover image region, and further changes are not discernible although leaves still grow. Earlier studies investigating the relationship between leaf traits and GCC have found a decoupling of GCC from other leaf traits (Keenan et al., 2014; Yang et al. 2014). Keenan et al. (2014) explained GCC development, showing that GCC becomes insensitive to LAI increases at high LAI, and thus LAI peaks later than GCC. Leaves also change color during their development. During some years at some sites we observed a pronounced peak of GCC after the leaf unfolding and maturation period, which quickly declined to summer level and further but gradually decreased towards autumn, implying that methods need elaboration to account for the unexpected behaviour. This behaviour

585 obviously cannot be properly captured by the double exponential fit, which assumed steady decline of
586 GCC until DD. Elaboration of methods further could benefit from a priori information about plausible
587 season end range. The causes of this peak are unclear, but it could be related to the distinctive light
588 green colour of new leaves, which is subsequently lost with increasing chlorophyll packing to the leaves
589 along with albedo decrease within high chlorophyll contents (Bray et al., 1966), and possibly due to
590 changes of leaf surface due to aging. Yang et al. (2014) observed that the chlorophyll peak lags 20 days
591 behind the GCC peak in white oaks, which could explain the quick decline after the peak. The reasons for
592 the variable GCC response among the sites and years remain unclear. In previous studies, variants of the
593 double exponential fits (Elmore et al., 2014; Klosterman et al., 2014) occasionally caught the summer
594 peak appropriately but then failed for other cases, which could be partially related to this issue.
595
596 Reflectance analyses, such as those conducted with cameras, are sensitive to the spectral distribution of
597 the exposing radiation. A humped GCC pattern peaking at midday detected by Ahrends et al (2008), may
598 be an indication of temporal differences in exposing light angle and colour, but it may be due to a low
599 light exposure of objects that may render GCC analyses unreliable under low light (Sonnentag et al.,
600 2012). Linkosalmi et al. (2016) excluded the dark winter days from the image data series analysed when
601 they analysed an image time series of Scots pine (10.5281/zenodo.815481) and wetland
602 (10.5281/zenodo.815485) north from Arctic Circle. Our results, on the other hand, were preconditioned
603 by the exclusion of pixels with a poor exposure of any of the colour channels (digital number < 30), and
604 by limiting the images used for the period between 08:00-16:00. Due to this filter, some of the darkest
605 days were completely excluded at the northernmost sites. Our filter additionally causes the pixel
606 number within ROI to vary with illumination, but this did not seem to be a significant factor. Therefore,
607 we consider that our filtering cleaned the GCC time series from (any potential) systematic variation in
608 GCC, leaving only residual variation that is too small to bias the image analysis and can be party
609 explained by day-to-day variability in light conditions, e.g. due to cloud cover.

610

611 *Conclusions*

612

613 Our results extend the earlier conclusions that the camera-based phenology analysis provides a sound
614 method for quantitative monitoring of phenology (e.g. Richardson, et al., 2007; Ahrends et al., 2008).
615 We used networked cameras from a long latitudinal transect to study the phenology of the most widely
616 spread deciduous species in the boreal zone, and showed that the cameras and targets provide reliable
617 predictions of the seasonal development of birches in various conditions, particularly for season start
618 using GCC and season end when using RCC. Small image elements were useful for the analyses, but
619 analyses should account for their movement in wind, and in the longer term analyses, also tracking of
620 their growth.

621

622 Moreover, the established network, together with the image analysis methods adopted, provides a
623 good basis for automated monitoring of key phenological events for birch, which could reduce the costs
624 of field monitoring. Season start and end dates could also be informative for the forcing of carbon
625 balance models and in the calibration of phenology models, while we expect midseason transition dates
626 to be much harder to use. Further research is required to understand how the species-specific
627 phenological transitions are reflected in remote sensing phenology products (which typically aggregate
628 signals over wide areas) in spring including nearly simultaneously occurring snow cover changes in
629 northernmost areas. We consider that networks of modest density such as our network can cover the
630 phenology of a few dominant tree species in the region, and can thus provide a good basis for the
631 monitoring of species-specific phenology in the area.

632

5 Acknowledgements

With the contribution of the LIFE+ financial instrument of the European Union (LIFE12 ENV/FI/000409 Monimet, http://monimet.fmi.fi).

6 Appendixes

A. Regions of interest of image time series used in the phenological analyses of birch species.

   < APPEARS AS SEPARATE FILE IN SUBMISSION >

B. GCC time series, curve fits, and estimates of phenological transition dates (camera-based and visually interpreted).

   < APPEARS AS SEPARATE FILE IN SUBMISSION >

C. Data summary table and additional models of phenological transition dates.

< APPEARS AS SEPARATE FILE IN SUBMISSION >

7 References

Ahrends, H. E., Etzold, S., Kutsch, W. L., Stoeckli, R., Bruegger, R., Jeanneret, F., Wanner, H., Buchmann, N. and Eugster, W.: Tree phenology and carbon dioxide fluxes: use of digital photography for process-based interpretation at the ecosystem scale, Clim. Res., 39, 261-274, 2009.

Ahrends, H. E., Brügger, R., Stöckli, R., Schenk, J., Michna, P., Jeanneret, F., Wanner, H. and Eugster, W.: Quantitative phenological observations of a mixed beech forest in northern Switzerland with digital photography, Journal of Geophysical Research: Biogeosciences, 113, 2008.

Arslan, A. N., Tanis, C. M., Metsämäki, S., Aurela, M., Böttcher, K., Linkosalmi, M. and Peltoniemi, M.: Automated Webcam Monitoring of Fractional Snow Cover in Northern Boreal Conditions. Geosciences, 7, 55, 2017.

Badeck, F., Bondeau, A., Böttcher, K., Doktor, D., Lucht, W., Schaber, J. and Sitch, S.: Responses of spring phenology to climate change, New Phytol., 162, 295-309, 2004.

Basler, D.: Evaluating phenological models for the prediction of leaf-out dates in six temperate tree species across central Europe, Agric. For. Meteorol., 217, 10-21, 2016.

Böttcher, K., Aurela, M., Kervinen, M., Markkanen, T., Mattila, O., Kolari, P., Metsämäki, S., Aalto, T., Arslan, A. N. and Pulliainen, J.: MODIS time-series-derived indicators for the beginning of the growing season in boreal coniferous forest — A comparison with CO2 flux measurements and phenological observations in Finland, Remote Sens. Environ., 140, 625-638, 2014.

Bray, J. R., Sanger, J. E. and Archer, A. L.: The Visible Albedo of Surfaces in Central Minnesota, Ecology, 47, 524-531, 1966.

667 Delbart, N., Picard, G., Le Toan, T., Kergoat, L., Quegan, S., Woodward, I., Dye, D. and Fedotova, V.:
668 Spring phenology in boreal Eurasia over a nearly century time scale, Global Change Biol., 14, 603-614,
669 2008.

670 Elmore, A. J., Guinn, S. M., Minsley, B. J. and Richardson, A. D.: Landscape controls on the timing of
671 spring, autumn, and growing season length in mid-Atlantic forests, Global Change Biol., 18, 656-674,
672 2012.

673 Filippa, G., Cremonese, E., Migliavacca, M., Galvagno, M., Forkel, M., Wingate, L., Tomelleri, E., Morra di
674 Cella, U. and Richardson, A. D.: Phenopix: A R package for image-based vegetation phenology, Agric. For.
675 Meteorol., 220, 141-150, 2016.

676 Forkel, M. and Wutzler, T.: greenbrown - land surface phenology and trend analysis. A package for the R
677 software., Version 2.2, 2015-04-15, 2015.

678 Forkel, M., Migliavacca, M., Thonicke, K., Reichstein, M., Schaphoff, S., Weber, U. and Carvalhais, N.:
679 Codominant water control on global interannual variability and trends in land surface phenology and
680 greenness, Global Change Biol., 21, 3414-3435, 2015.

681 Garvelmann, J., Pohl, S. and Weiler, M.: From observation to the quantification of snow processes with a
682 time-lapse camera network, Hydrology and Earth System Sciences, 17, 1415-1429, 2013.

683 Gonsamo, A. and Chen, J. M.: Circumpolar vegetation dynamics product for global change study,
684 Remote Sens. Environ., 182, 13-26, 2016.

685 Gu, L., Post, W. M., Baldocchi, D. D., Black, T. A., Suyker, A. E., Verma, S. B., Vesala, T. and Wofsy, S. C.:
686 Characterizing the Seasonal Dynamics of Plant Community Photosynthesis Across a Range of Vegetation
687 Types, in: Phenology of Ecosystem Processes: Applications in Global Change Research, Noormets, A.
688 (Ed.), Springer New York, New York, NY, 35-58, 2009.

689 Häkkinen, R.: Analysis of bud-development theories based on long-term phenological and air
690 temperature time series: application to Betula sp. leaves. thesis/masters, Finnish Forest Research
691 Institute, 1999.

692 Hogg, E. H., Price, D. T. and Black, T. A.: Postulated Feedbacks of Deciduous Forest Phenology on
693 Seasonal Climate Patterns in the Western Canadian Interior, J. Climate, 13, 4229-4243, 2000.

694 Hufkens, K., Friedl, M., Sonnentag, O., Braswell, B. H., Milliman, T. and Richardson, A. D.: Linking near-
695 surface and satellite remote sensing measurements of deciduous broadleaf forest phenology, Remote
696 Sens. Environ., 117, 307-321, 2012.

697 Jeong, S., Ho, C., Gim, H. and Brown, M. E.: Phenology shifts at start vs. end of growing season in
698 temperate vegetation over the Northern Hemisphere for the period 1982-2008, Global Change Biol., 17,
699 2385-2399, 2011.

700 Jönsson, A. M., Eklundh, L., Hellström, M., Bärring, L. and Jönsson, P.: Annual changes in MODIS
701 vegetation indices of Swedish coniferous forests in relation to snow dynamics and tree phenology,
702 Remote Sens. Environ., 114, 2719-2730, 2010.

703 Karlsen, S. R., Tolvanen, A., Kubin, E., Poikolainen, J., Høgda, K. A., Johansen, B., Danks, F. S., Aspholm,
704 P., Wielgolaski, F. E. and Makarova, O.: MODIS-NDVI-based mapping of the length of the growing season
705 in northern Fennoscandia, International Journal of Applied Earth Observation and Geoinformation, 10,
706 253-266, 2008.

707 Keenan, T. F., Baker, I., Barr, A., Ciais, P., Davis, K., Dietze, M., Dragoni, D., Gough, C. M., Grant, R.,
708 Hollinger, D., Hufkens, K., Poulter, B., McCaughey, H., Raczka, B., Ryu, Y., Schaefer, K., Tian, H., Verbeeck,
709 H., Zhao, M. and Richardson, A. D.: Terrestrial biosphere model performance for inter-annual variability
710 of land-atmosphere CO2 exchange, Global Change Biol., 18, 1971-1987, 2012.

711 Keenan, T. F., Darby, B., Felts, E., Sonnentag, O., Friedl, M. A., Hufkens, K., O'Keefe, J., Klosterman, S.,
712 Munger, J. W., Toomey, M. and Richardson, A. D.: Tracking forest phenology and seasonal physiology
713 using digital repeat photography: a critical assessment, Ecol. Appl., 24, 1478-1489, 2014.

714 Klosterman, S. T., Hufkens, K., Gray, J. M., Melaas, E., Sonnentag, O., Lavine, I., Mitchell, L., Norman, R.,
715 Friedl, M. A. and Richardson, A. D.: Evaluating remote sensing of deciduous forest phenology at multiple
716 spatial scales using PhenoCam imagery, Biogeosciences, 11, 4305-4320, 2014.

717 Kubin, E., Kotilainen, E., Poikolainen, J., Hokkanen, T., Nevalainen, S., Pouttu, A., Karhu, J. and Pasanen,
718 J.: Monitoring instructions of the Finnish national phenological network, Finnish Forest Research
719 Institute, Muhos Research Unit, 2007.

720 Liang, L., Schwartz, M. D. and Fei, S.: Validating satellite phenology through intensive ground
721 observation and landscape scaling in a mixed seasonal forest, Remote Sens. Environ., 115, 143-157,
722 2011.

723 Linkosalmi, M., Aurela, M., Tuovinen, J. -P., Peltoniemi, M., Tanis, C. M., Arslan, A. N., Kolari, P.,
724 Böttcher, K., Aalto, T., Rainne, J., Hatakka, J. and Laurila, T.: Digital photography for assessing the link
725 between vegetation phenology and CO2 exchange in two contrasting northern ecosystems,
726 Geoscientific Instrumentation, Methods and Data Systems, 5, 417-426, 2016.

727 Linkosalo, T., Lappalainen, H. K. and Hari, P.: A comparison of phenological models of leaf bud burst and
728 flowering of boreal trees using independent observations, Tree Physiology, 28, 1873-1882, 2008.

729 Liu, L., Liang, L., Schwartz, M. D., Donnelly, A., Wang, Z., Schaaf, C. B. and Liu, L.: Evaluating the potential
730 of MODIS satellite data to track temporal dynamics of autumn phenology in a temperate mixed forest,
731 Remote Sens. Environ., 160, 156-165, 2015.

732 Menzel, A. and Fabian, P.: Growing season extended in Europe, Nature, 397, 659-659, 1999.

733 Menzel, A., Sparks, T. H., Estrella, N., Koch, E., Aasa, A., Ahas, R., Alm-Kübler, K., Bissolli, P., Braslavská,
734 O., Briede, A., Chmielewski, F. M., Crepinsek, Z., Curnel, Y., Dahl, Å., Defila, C., Donnelly, A., Filella, Y.,
735 Jatczak, K., Måge, F., Mestre, A., Nordli, Ø., Peñuelas, J., Pirinen, P., Remisová, V., Scheifinger, H., Striz,
736 M., Susnik, A., Van Vliet, A. J. H., Wielgolaski, F., Zach, S. and Zust, A.: European phenological response to
737 climate change matches the warming pattern, Global Change Biol., 12, 1969-1976, 2006.

738 Metsämäki, S., Pulliainen, J., Salminen, M., Luojus, K., Wiesmann, A., Solberg, R., Böttcher, K., Hiltunen,
739 M. and Ripper, E.: Introduction to GlobSnow Snow Extent products with considerations for accuracy
740 assessment, Remote Sens. Environ., 156, 96-108, 2015.

741 Migliavacca, M., Sonnentag, O., Keenan, T. F., Cescatti, A., O'Keefe, J. and Richardson, A. D.: On the
742 uncertainty of phenological responses to climate change, and implications for a terrestrial biosphere
743 model, Biogeosciences, 9, 2063-2083, 2012.

744 Migliavacca, M., Galvagno, M., Cremonese, E., Rossini, M., Meroni, M., Sonnentag, O., Cogliati, S.,
745 Manca, G., Diotri, F., Busetto, L., Cescatti, A., Colombo, R., Fava, F., Morra di Cella, U., Pari, E., Siniscalco,
746 C. and Richardson, A. D.: Using digital repeat photography and eddy covariance data to model grassland
747 phenology and photosynthetic CO2 uptake, Agric. For. Meteorol., 151, 1325-1337, 2011.

748 Mizunuma, T., Wilkinson, M., L. Eaton, E., Mencuccini, M., I. L. Morison, J. and Grace, J.: The relationship
749 between carbon dioxide uptake and canopy colour from two camera systems in a deciduous forest in
750 southern England, Funct. Ecol., 27, 196-207, 2013.

751 Nagai, S., Saitoh, T. M., Kobayashi, H., Ishihara, M., Suzuki, R., Motohka, T., Nasahara, K. N. and
752 Muraoka, H.: In situ examination of the relationship between various vegetation indices and canopy
753 phenology in an evergreen coniferous forest, Japan, Int. J. Remote Sens., 33, 6202-6214, 2012.

754 Peichl, M., Sonnentag, O. and Nilsson, M. B.: Bringing Color into the Picture: Using Digital Repeat
755 Photography to Investigate Phenology Controls of the Carbon Dioxide Exchange in a Boreal Mire,
756 Ecosystems, 18, 115-131, 2015.

757 Peltoniemi, M., Aurela, M., Böttcher, K., Kolari, P., Loehr, J., Karhu, J., Linkosalmi, M., Tanis, C. M.,
758 Tuovinen, J. -P. and Arslan, A. N.: Webcam network and image database for studies of phenological
759 changes of vegetation and snow cover in Finland, image time series from 2014--2016, Earth System
760 Science Data Discussions, 2017, 1-23, 2017.

761 Pinheiro, J., Bates, D., DebRoy, S. and Sarkar, D. R.: nlme: Linear and Nonlinear Mixed Effects Models, R
762 package, version 3.1-122, 2015.

763 Poikolainen, J., Karhu, J. and Kubin, E.: Development of a plant-phenological observation network in
764 Finland., Finnish Forest Research Institute, Research Papers, 623, 97-101, 1996.

765 Pudas, E., Leppälä, M., Tolvanen, A., Poikolainen, J., Venäläinen, A. and Kubin, E.: Trends in phenology of
766 Betula pubescens across the boreal zone in Finland, Int. J. Biometeorol., 52, 251-259, 2008.

767 R Core Team: R: A Language and Environment for Statistical Computing, R Foundation for Statistical
768 Computing, Vienna, Austria, 2015.

769 Ranta, H., Hokkanen, T., Linkosalo, T., Laukkanen, L., Bondestam, K. and Oksanen, A.: Male flowering of
770 birch: Spatial synchronization, year-to-year variation and relation of catkin numbers and airborne pollen
771 counts, For. Ecol. Manage., 255, 643-650, 2008.

772 Richardson, A. D., Anderson, R. S., Arain, M. A., Barr, A. G., Bohrer, G., Chen, G., Chen, J. M., Ciais, P.,
773 Davis, K. J., Desai, A. R., Dietze, M. C., Dragoni, D., Garrity, S. R., Gough, C. M., Grant, R., Hollinger, D. Y.,
774 Margolis, H. A., McCaughey, H., Migliavacca, M., Monson, R. K., Munger, J. W., Poulter, B., Raczka, B. M.,
775 Ricciuto, D. M., Sahoo, A. K., Schaefer, K., Tian, H., Vargas, R., Verbeeck, H., Xiao, J. and Xue, Y.:

776 Terrestrial biosphere models need better representation of vegetation phenology: results from the
777 North American Carbon Program Site Synthesis, Global Change Biol., 18, 566-584, 2012.

778 Richardson, A. D., Braswell, B. H., Hollinger, D. Y., Jenkins, J. P. and Ollinger, S. V.: Near-surface remote
779 sensing of spatial and temporal variation in canopy phenology, Ecol. Appl., 19, 1417-1428, 2009.

780 Richardson, A. D., Jenkins, J. P., Braswell, B. H., Hollinger, D. Y., Ollinger, S. V. and Smith, M.: Use of
781 digital webcam images to track spring green-up in a deciduous broadleaf forest, Oecologia, 152, 323-
782 334, 2007.

783 Richardson, A. D., Keenan, T. F., Migliavacca, M., Ryu, Y., Sonnentag, O. and Toomey, M.: Climate
784 change, phenology, and phenological control of vegetation feedbacks to the climate system, Agric. For.
785 Meteorol., 169, 156-173, 2013.

786 Rousi, M. and Pusenius, J.: Variations in phenology and growth of European white birch (Betula pendula)
787 clones, Tree Physiology, 25, 201-210, 2005.

788 Ruosteenoja, K., Jylhä, K. and Kämäräinen, M.: Climate Projections for Finland Under the RCP Forcing
789 Scenarios, Geophysica, 51, 17-50, 2016.

790 Saitoh, T. M., Nagai, S., Saigusa, N., Kobayashi, H., Suzuki, R., Nasahara, K. N. and Muraoka, H.: Assessing
791 the use of camera-based indices for characterizing canopy phenology in relation to gross primary
792 production in a deciduous broad-leaved and an evergreen coniferous forest in Japan, Ecological
793 Informatics, 11, 45-54, 2012.

794 Salvatori, R., Plini, P., Giusto, M., Valt, M., Salzano, R., Montagnoli, M., Cagnati, A., Crepaz, G. and
795 Sigismondi, D.: Snow cover monitoring with images from digital camera systems, Italian Journal of
796 Remote Sensing, 43 (2), 137-145, 2011.

797 Siljamo, P., Sofiev, M., Ranta, H., Linkosalo, T., Kubin, E., Ahas, R., Genikhovich, E., Jatczak, K., Jato, V.,
798 Nekovář, J., Minin, A., Severova, E. and Shalaboda, V.: Representativeness of point-wise phenological
799 Betula data collected in different parts of Europe, Global Ecol. Biogeogr., 17, 489-502, 2008.

800 Sonnentag, O., Hufkens, K., Teshera-Sterne, C., Young, A. M., Friedl, M., Braswell, B. H., Milliman, T.,
801 O'Keefe, J. and Richardson, A. D.: Digital repeat photography for phenological research in forest
802 ecosystems, Agric. For. Meteorol., 152, 159-177, 2012.

803 Venäläinen, A., Tuomenvirta, H., Pirinen, P. and Drebs, A.: A basic Finnish climate data set 1961–2000-
804 description and illustration, Finnish Meteorological Institute Reports, 2005:5, 1-27, 2005.

805 Westergaard-Nielsen, A., Lund, M., Hansen, B. U. and Tamstorf, M. P.: Camera derived vegetation
806 greenness index as proxy for gross primary production in a low Arctic wetland area, ISPRS Journal of
807 Photogrammetry and Remote Sensing, 86, 89-99, 2013.

808 Wingate, L., Ogée, J., Cremonese, E., Filippa, G., Mizunuma, T., Migliavacca, M., Moisy, C., Wilkinson, M.,
809 Moureaux, C., Wohlfahrt, G., Hammerle, A., Hörtnagl, L., Gimeno, C., Porcar-Castell, A., Galvagno, M.,
810 Nakaji, T., Morison, J., Kolle, O., Knohl, A., Kutsch, W., Kolari, P., Nikinmaa, E., Ibrom, A., Gielen, B.,
811 Eugster, W., Balzarolo, M., Papale, D., Klumpp, K., Köstner, B., Grünwald, T., Joffre, R., Ourcival, J.,
812 Hellstrom, M., Lindroth, A., George, C., Longdoz, B., Genty, B., Levula, J., Heinesch, B., Sprintsin, M.,
813 Yakir, D., Manise, T., Guyon, D., Ahrends, H., Plaza-Aguilar, A., Guan, J. H. and Grace, J.: Interpreting
814 canopy development and physiology using a European phenology camera network at flux sites,
815 Biogeosciences, 12, 5995-6015, 2015.

816 Yang, X., Tang, J. and Mustard, J. F.: Beyond leaf color: Comparing camera-based phenological metrics
817 with leaf biochemical, biophysical, and spectral properties throughout the growing season of a
818 temperate deciduous forest, Journal of Geophysical Research: Biogeosciences, 119, 181-191, 2014.

819 Zamorano, J. G., Hokkanen, T. and Lehikoinen, A.: Climate-driven synchrony in seed production of
820 masting deciduous and conifer tree species, Journal of Plant Ecology, rtw117, 2016.

821 Zhang, X., Friedl, M. A. and Schaaf, C. B.: Global vegetation phenology from Moderate Resolution
822 Imaging Spectroradiometer (MODIS): Evaluation of global patterns and comparison with in situ
823 measurements, Journal of Geophysical Research: Biogeosciences, 111, G04017, 2006.

824 Zhao, J., Zhang, H., Zhang, Z., Guo, X., Li, X. and Chen, C.: Spatial and Temporal Changes in Vegetation
825 Phenology at Middle and High Latitudes of the Northern Hemisphere over the Past Three Decades,
826 Remote Sensing, 7, 10973-10995, 2015.

8 Figure captions

Figure 1 Locations of sites and cameras and phenological field monitoring plots used in the study.

Figure 2 Phenological data from Lammi site (for other sites, see Suppl. B). Top panel: horizontal black lines refer to visually determined phenological periods from image time periods. Bottom panel: radiation and air Temperature (T) are 5 day running means. Temperature sums are calculated from daily mean T with 0 °C threshold (starting from 21st Mar), and with 5 °C threshold (from 1st Jan).

Figure 3 Comparison of phenological transition dates. X-axes values (see Table 2) were extracted automatically from image time series based on cubic spline fits and y-axes values from the same plots were based on the visual examination of image time series. The solid line is the fitted regression line, and dash-dot line is 1:1 line. Each site has 1-3 observation years (indicated by different colors). Panel d: gray symbols indicate visual observation of 10% leaves fallen.

Figure 4 Comparison of phenological transition dates estimated based on double exponential fits (Gu et al., 2009) to GCC (X-axis). See Figure 3 for legends and other explanations.

Figure 5 Comparison of phenological transition dates for end of season dates based on GCC (EOS) with the visual estimates. See Figure 3 for legends and other explanations.

Figure 6 Fitted splines and extracted phenological transition dates in a South to North (top to bottom) gradient in Finland. SOS dates (upwards triangles, △) were determined from GCC spline fits and EOSr dates (downwards triangle, ▽) from peaks of autumn RCC.

Figure 7 Latitudinal gradients in key phenological dates and measurements of corresponding variables in the field. Regression functions are in Table 6. Year did not significantly interact with latitude in the models, indicating no slope differences between the years.

Figure 1

Click here to download high resolution image

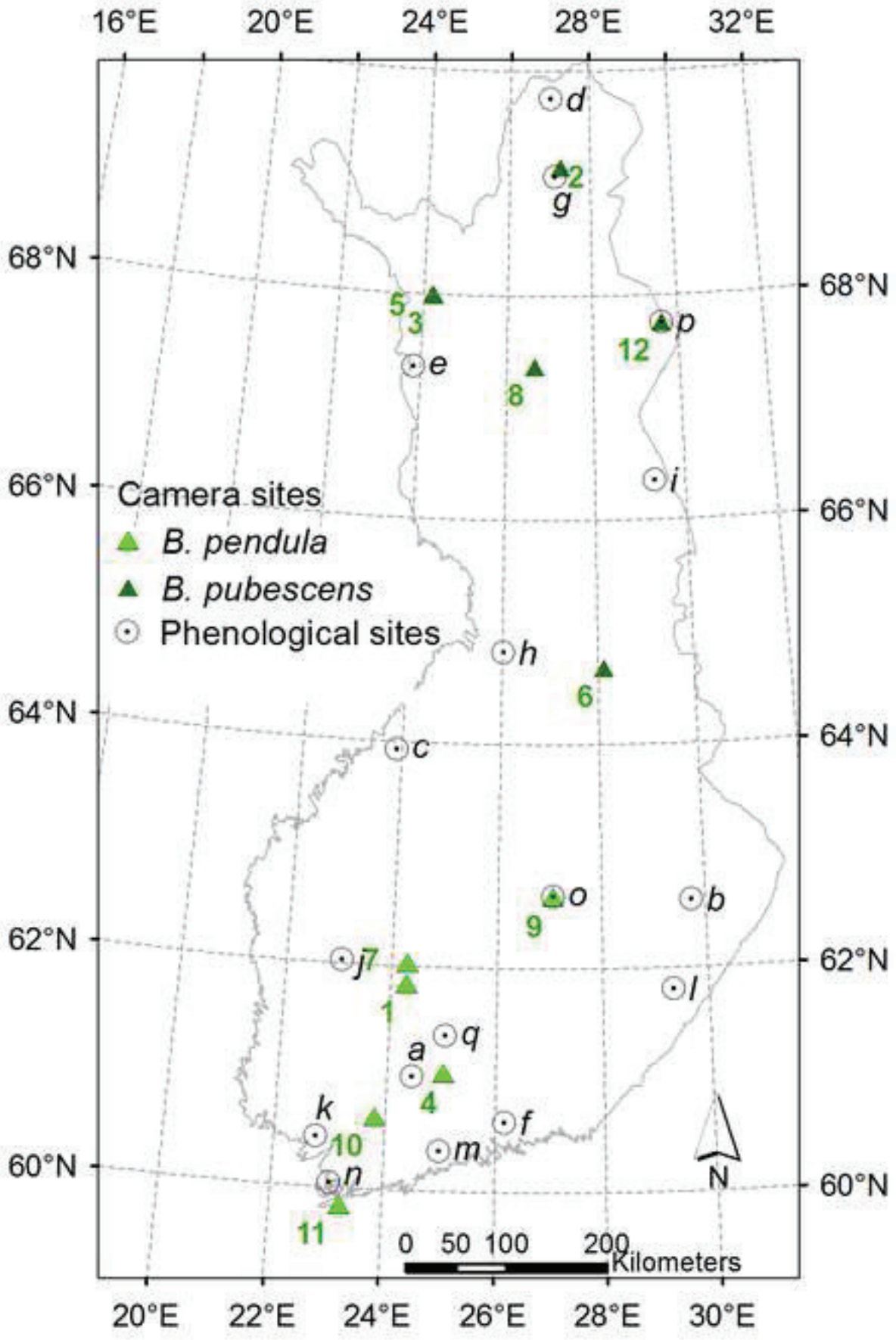

Figure 2

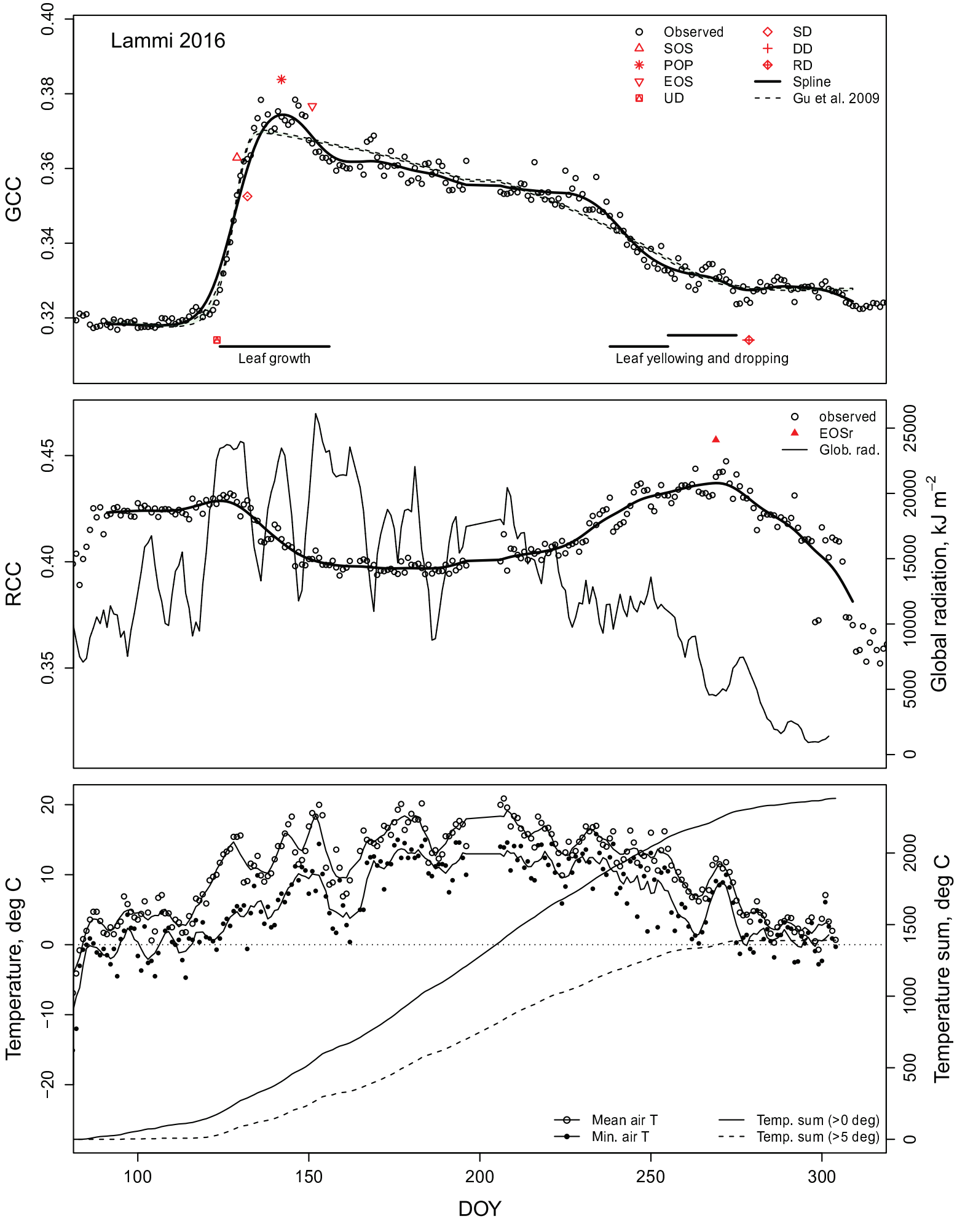
Lammi 2016
Observed
SOS
POP
EOS
UD
SD
DD
RD
Spline
Gu et al. 2009
GCC
Leaf growth
Leaf yellowing and dropping
observed
EOSr
Glob. rad.
RCC
Global radiation, kJ m^{-2}
Mean air T
Min. air T
Temp. sum (>0 deg)
Temp. sum (>5 deg)
Temperature, deg C
Temperature sum, deg C
DOY

Figure 3

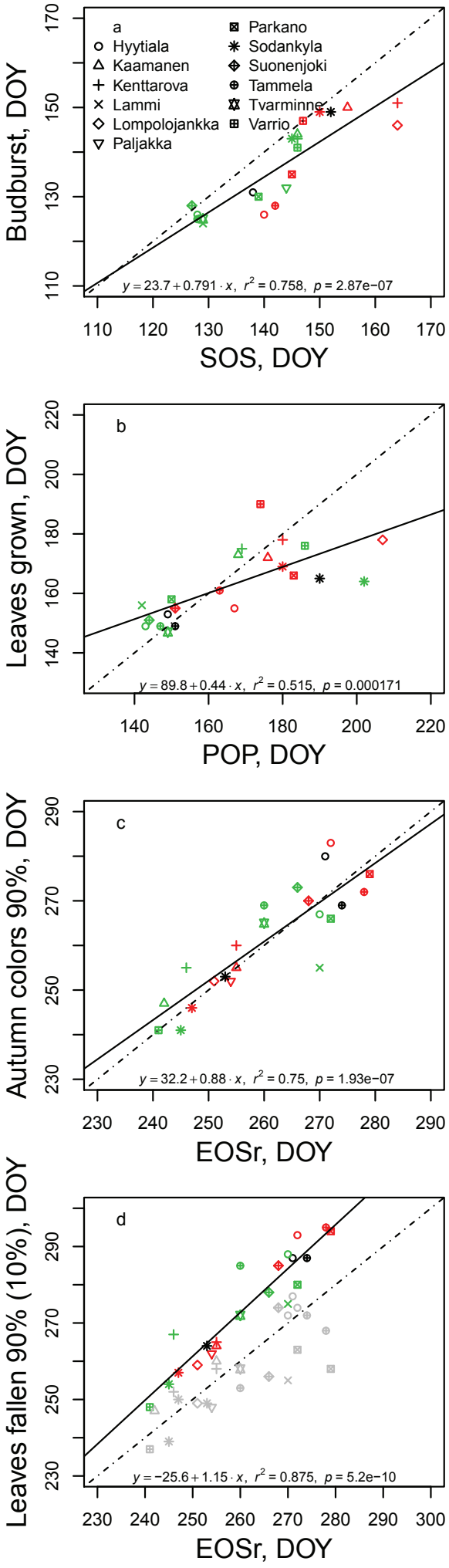
a
Hyytiala
Kaamanen
Kenttarova
Lammi
Lompolojankka
Paljakka
Parkano
Sodankyla
Suonenjoki
Tammela
Tvarminne
Varrio
Budburst, DOY
SOS, DOY
y = 23.7 + 0.791 · x, r² = 0.758, p = 2.87e−07
b
Leaves grown, DOY
POP, DOY
y = 89.8 + 0.44 · x, r² = 0.515, p = 0.000171
c
Autumn colors 90%, DOY
EOSr, DOY
y = 32.2 + 0.88 · x, r² = 0.75, p = 1.93e−07
d
Leaves fallen 90% (10%), DOY
EOSr, DOY
y = −25.6 + 1.15 · x, r² = 0.875, p = 5.2e−10

Figure 4

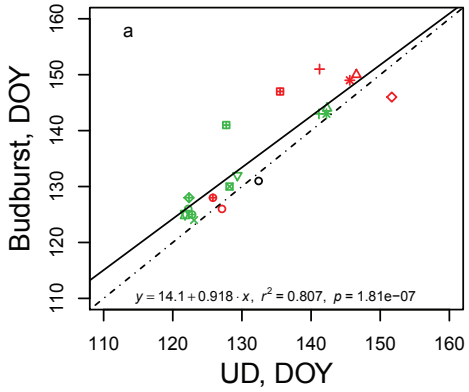
a
Budburst, DOY
UD, DOY
y = 14.1 + 0.918 · x, r² = 0.807, p = 1.81e−07
110
120
130
140
150
160

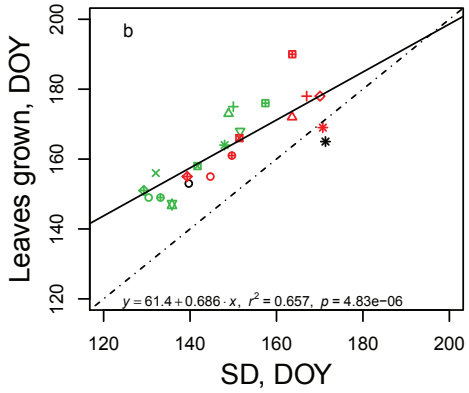
b
Leaves grown, DOY
SD, DOY
y = 61.4 + 0.686 · x, r² = 0.657, p = 4.83e−06
120
140
160
180
200

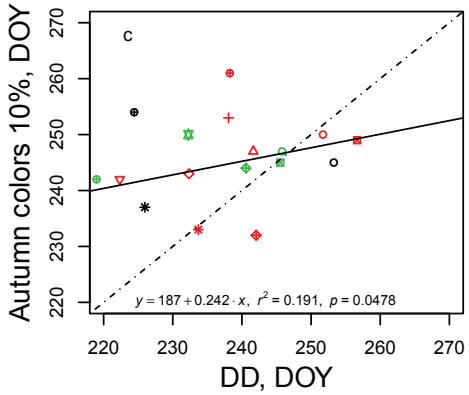
c
Autumn colors 10%, DOY
DD, DOY
y = 187 + 0.242 · x, r² = 0.191, p = 0.0478
220
230
240
250
260
270

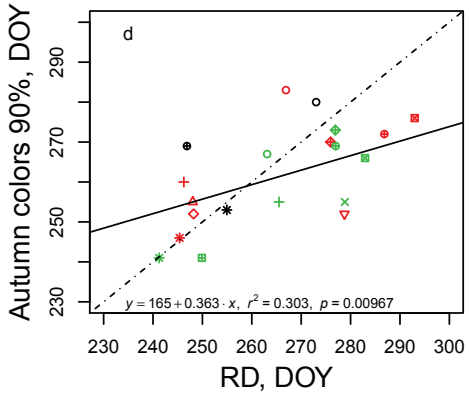
d
Autumn colors 90%, DOY
RD, DOY
y = 165 + 0.363 · x, r² = 0.303, p = 0.00967
230
240
250
260
270
280
290
300

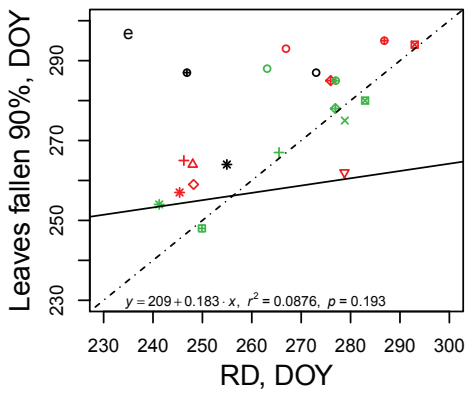
e
Leaves fallen 90%, DOY
RD, DOY
y = 209 + 0.183 · x, r² = 0.0876, p = 0.193
230
240
250
260
270
280
290
300

Figure 5

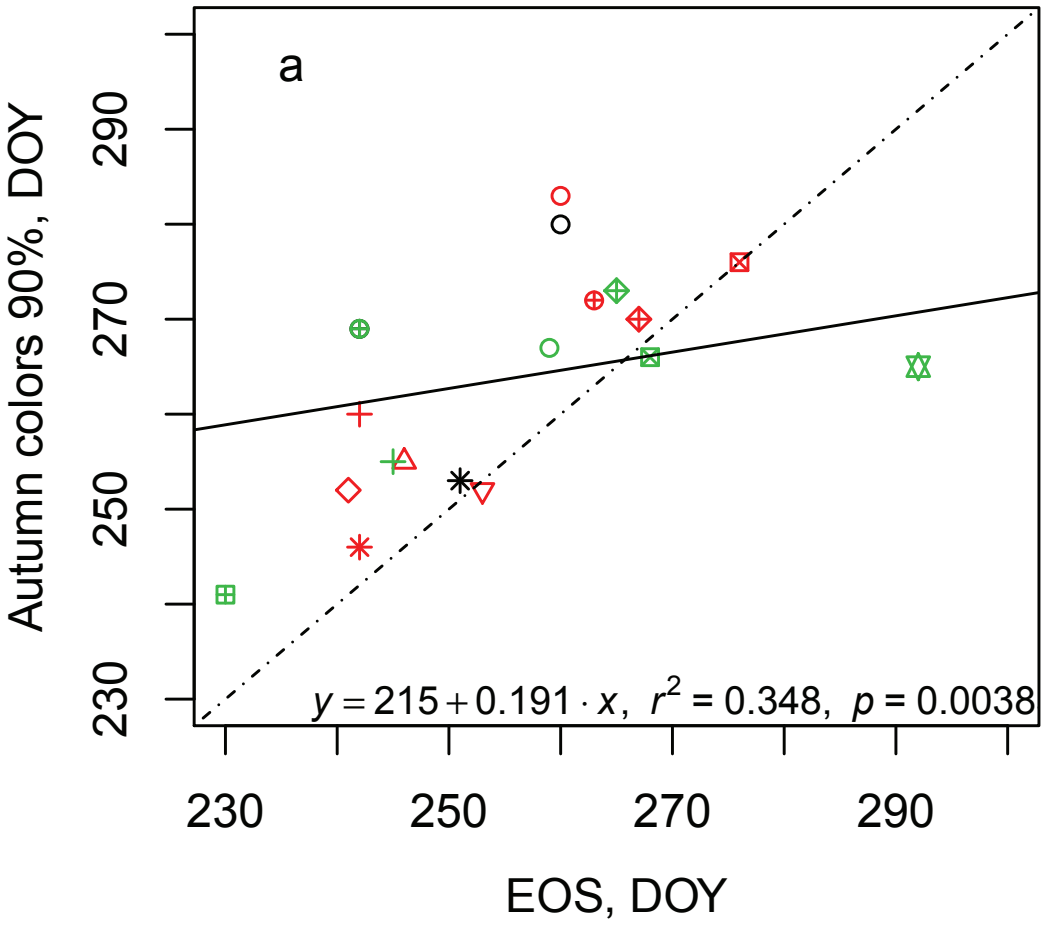
a
Autumn colors 90%, DOY
230
250
270
290
$y = 215 + 0.191 \cdot x$, $r^2 = 0.348$, $p = 0.0038$
230
250
270
290
EOS, DOY

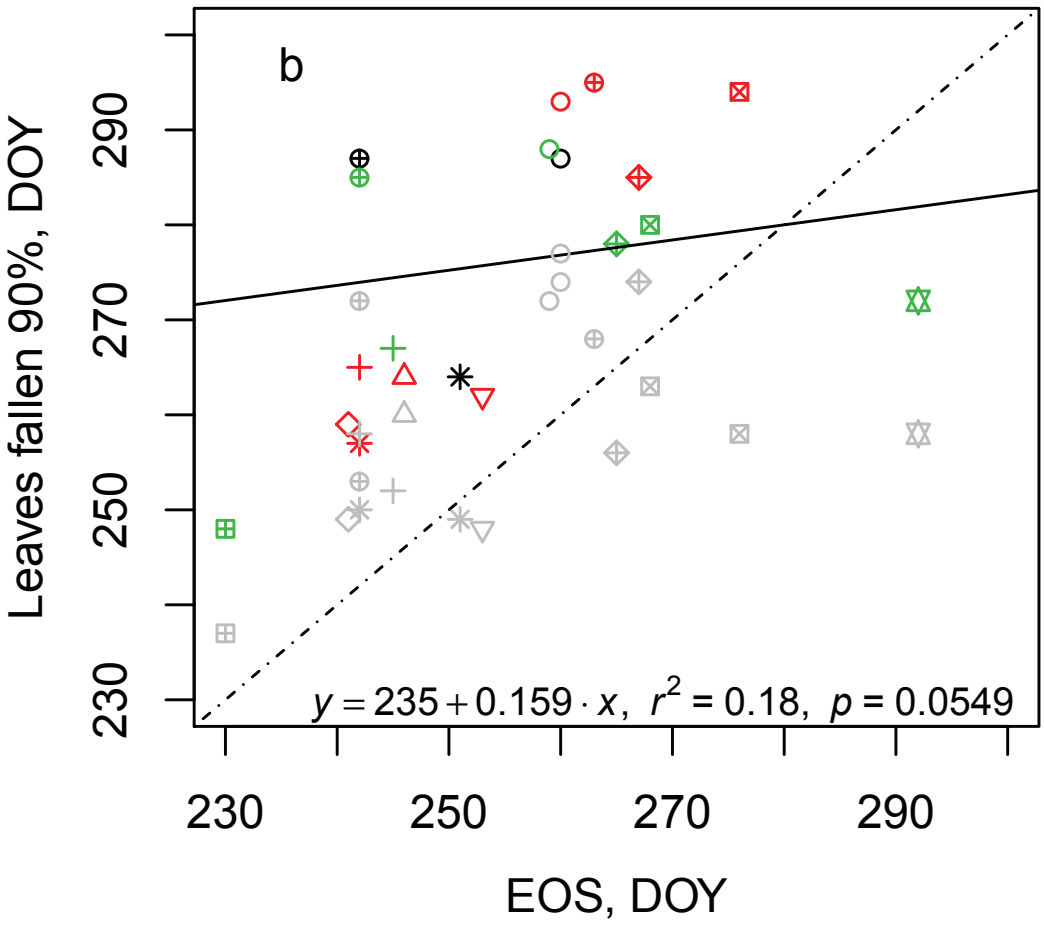
b
Leaves fallen 90%, DOY
230
250
270
290
$y = 235 + 0.159 \cdot x$, $r^2 = 0.18$, $p = 0.0549$
230
250
270
290
EOS, DOY

Figure 6

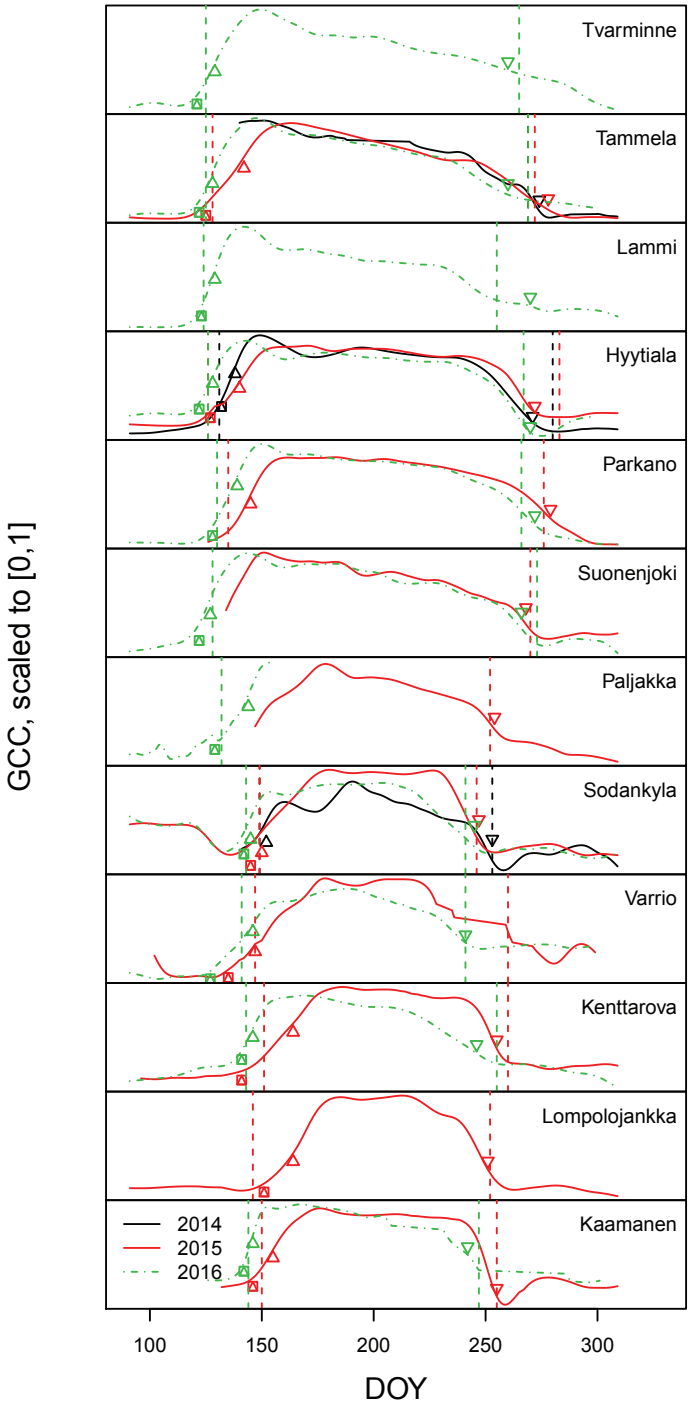
Tvarminne
Tammela
Lammi
Hyytiala
Parkano
Suonenjoki
Paljakka
Sodankyla
Varrio
Kenttarova
Lompolojankka
Kaamanen
2014
2015
2016
GCC, scaled to [0,1]
100
150
200
250
300
DOY

Figure 7

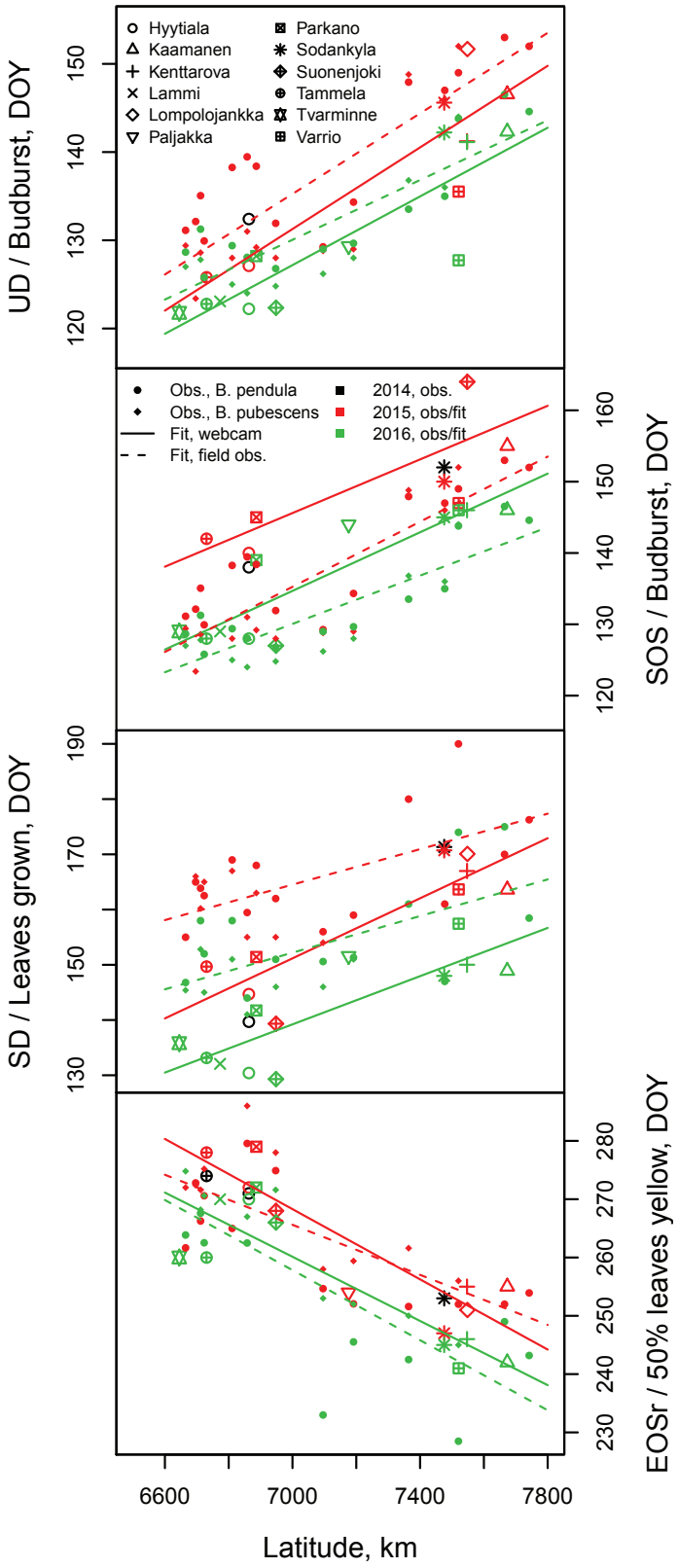
Hyytiala
Kaamanen
Kenttarova
Lammi
Lompolojankka
Paljakka
Parkano
Sodankyla
Suonenjoki
Tammela
Tvarminne
Varrio
Obs., B. pendula
Obs., B. pubescens
Fit, webcam
Fit, field obs.
2014, obs.
2015, obs/fit
2016, obs/fit
UD / Budburst, DOY
SOS / Budburst, DOY
SD / Leaves grown, DOY
EOSr / 50% leaves yellow, DOY
Latitude, km
6600
7000
7400
7800